

Nanoimaging Cells Using Soft X-Ray Tomography

Dilworth Y. Parkinson, Lindsay R. Epperly, Gerry McDermott,
Mark A. Le Gros, Rosanne M. Boudreau, and Carolyn A. Larabell

Abstract

Soft X-ray microscopy is ideally suited to visualizing and quantifying biological cells. Specimens, including eukaryotic cells, are imaged intact, unstained and fully hydrated, and therefore visualized in a near-native state. The contrast in soft X-ray microscopy is generated by the differential attenuation of X-rays by the molecules in the specimen—water is relatively transmissive to this type of illumination compared to carbon and nitrogen. The attenuation of X-rays by the specimen follows the Beer–Lambert law, and therefore both linear and a quantitative measure of thickness and chemical species present at each point in the cell. In this chapter, we will describe the procedures and computational methods that lead to 50 nm (or better) tomographic reconstructions of cells using soft X-ray microscope data, and the subsequent segmentation and analysis of these volumetric reconstructions. In addition to being a high-fidelity imaging modality, soft X-ray tomography is relatively high-throughput; a complete tomographic data set can be collected in a matter of minutes. This new modality is being applied to imaging cells that range from small prokaryotes to stem cells obtained from mammalian tissues.

Key words: Cell structure, Microscopy, Nanoimaging, Reconstruction, Soft X-ray tomography, Segmentation, Visualization

1. Introduction

Soft X-ray tomography (SXT) is a relatively recent addition to the spectacular array of imaging techniques available to biologists (1). As with all modalities, SXT fills a niche as being the optimal imaging technique for answering a particular set of questions (2). Specifically, SXT is uniquely suited to high-resolution, quantitative imaging of cells that are intact, unstained and fully hydrated—in other words, SXT excels at visualizing cells, including eukaryotic cells, that are held in a near-native state, and are, therefore, highly representative of the *in vivo* fully functional cell (1, 2).

The interior of a cell is highly organized and finely structured (1). This is especially true in the case of eukaryotic cells that are

partitioned into functionally discrete subcellular spaces termed organelles (3–5). In a 2-dimensional projection image of a cell these structural features are superimposed, making interpretation difficult, if not impossible. As a consequence, the subcellular architecture must be imaged in 3-dimensions. Since microscopes can only produce 2-dimensional images this may appear at first sight to be a major hurdle. However, in practice it is a relatively straightforward process to calculate 3-dimensional views from 2-dimensional data by the application of methods such as deconvolution or tomography (6). In the case of tomography, this simply means taking 2-dimensional images of the specimen from a number of different perspectives, usually at angular intervals around a rotation axis. Provided a sufficient number of images are taken, a fully isotropic, 3-dimensional representation of the specimen can be calculated from 2-dimensional imaging data (7). For SXT, a series (or “stack”) of images of the specimen are taken in this manner using a soft X-ray microscope (8). This contains all of the information necessary to calculate a volumetric reconstruction of the entire field of view over which imaging data was collected (9). In the case of small prokaryotic cells, the field of view may contain many tens or even hundreds of cells. For larger cells, such as eukaryotic cells, this number is obviously lower. For yeast, each field of view typically contains a maximum of six cells, and for higher order cells this will typically be a single cell. However, since SXT data collection is relatively rapid—standard exposure times for each image are on the order of 100 ms; a data set contains 90 or 180 images—the specimen throughput is still exceptionally high compared to other high-resolution cellular imaging modalities, even for large eukaryotic cells (9). Consequently, a large number of cells can be characterized in a relatively short space of time. For example, in two recently published studies quantifying yeast morphology, data from hundreds of high-resolution tomographic reconstructions were used in the analyses (5, 10). Neither of these types of nanoimaging studies could have been carried out using alternative techniques, such as electron tomography.

The specimen in SXT is illuminated using photons with energies that lie in the so-called water window region of the electromagnetic spectrum (11). The attenuation of these photons follows the Beer–Lambert Law, and is therefore linear, quantitative and dependent on chemical species and thickness. Carbon and nitrogen—major constituents of most biomolecules—attenuate the transmission of X-rays an order of magnitude more strongly than water (12). This characteristic produces exquisite contrast in SXT images of cells (5, 8, 13, 14). As a result, subcellular structures in an SXT reconstruction can be readily identified and “segmented” (i.e., isolated from the other contents in the reconstruction) based on their shape and the measured linear absorption coefficient (LAC) at each point in the cell (8, 12, 13, 15, 16)). Each organelle type

has a characteristic LAC. This reflects the organelle's biochemical composition. For example, yeast vacuoles have a low concentration of biomolecules and relatively high water content. Their LAC is, therefore, small compared with organelles that have low water content and are densely packed with biomolecules, for example the nucleus. The LAC values allow individual organelles to be identified and isolated, and provide key information on the internal structure of the organelle. Segmentation of the subcellular contents allows valuable quantitative analyses to be carried out. For example, it is easy to determine key parameters such as the volume and density of the organelles at key stages in the cell cycle, or how these parameters are affected by exposure to external influences, such as the presence or absence of specific molecules, temperature, confluence, and so on. This information is enormously valuable in studies ranging from basic cell biology to applied research aimed at generating new pharmaceuticals or in optimizing the economics of biofuel production.

We will now describe the methods and steps needed to image a sample of cells using SXT, beginning with specimen preparation.

2. Materials

Currently, soft X-ray microscopes are primarily located at synchrotron light sources. However, “table top” soft X-ray sources with suitable characteristics are being actively developed (17–19). We fully expect that in the near future soft X-ray microscopes using illumination from these types of small-scale sources will become commonplace in most research institutions.

Cell types suitable for SXT imaging span the entire spectrum of cell biology; from small bacteria cultured in the laboratory to large eukaryotic cells purified directly from primary mammalian tissue (1). The materials needed for the preparation of cells for soft X-ray microscopy are wide-ranging and highly specific to each cell type, and will, therefore, not be listed here. However, the following materials and instruments are in common use on the soft X-ray microscope XM-2 at the Advanced Light Source, Berkeley, CA (the optical layout of this microscope is shown in Fig. 1), and are generally useful for carrying out the technique irrespective of the photon source, or soft X-ray microscope design.

1. Brightfield Light Microscope: Zeiss Axiovert 40 CFL with Condenser 4.0 ($a=53$ mm) and Zeiss Objective A-Plan 10 \times /0.25 Ph 1.
2. Glass capillaries (Hilgenberg GmbH 1409190).
3. Quartz capillaries (Hilgenberg GmbH 1406785).

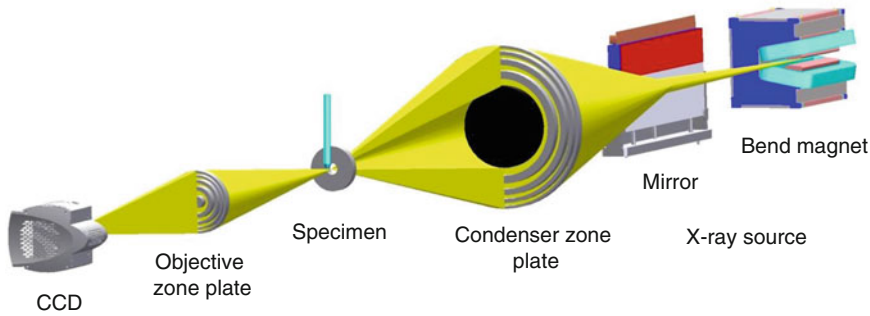


Fig. 1. Schematic representation of XM-2, a soft X-ray microscope for nanoimaging biological cells (located at the Advanced Light Source, Lawrence Berkeley National Laboratory, Berkeley, California). This is the first such microscope in the world to be built specifically for biological and biomedical research (for more information visit <http://ncxt.lbl.gov>).

4. Capillary tube puller (Sutter Instrument Co. Models P-97 & P-2000).
5. 100 nm colloidal gold nanoparticles (BB International, UK).
6. Filters: glue (Dow Corning 732 multipurpose sealant) and 20 and 15 μm sieves (BioDesign Cellmicrosieve).
7. Microloader tips (Eppendorf 930001007).
8. A multi-processor computer: Apple cluster with 20 nodes, each with two dual-core processors (see Note 1 for more details).
9. Image processing software: Matlab (Mathworks), ImageJ (National Institutes of Health, USA), XMIPP (Centro Nacional de Biotecnología, Madrid, Spain), ASPIRE (U. Michigan), and SPARX (Baylor College of Medicine) (see Note 2).
10. 3-D visualization and analysis software: Amira™ (Visage Imaging, Germany) and Avizo (VSG, France) (see Note 3).

3. Methods

3.1. Data Collection

3.1.1. Specimen Holders

When collecting imaging data for tomographic reconstruction the ideal specimen holder allows arbitrary access to a minimum of 180° of rotation (360° is even better). Use of grids and other mounting systems developed for electron microscopy hinders full rotation over angular ranges as large as these. Therefore, when possible it is preferable to use a mounting system such as thin-walled glass capillary tubes. In this chapter, we will only describe methods for imaging cells in glass or quartz capillary tubes. This approach allows full-rotation tomography, and gives optimum results. Capillary geometry allows data to be collected around a complete circle, and hence eliminates the issue of having to deal with the “missing wedge” of data inherent in other types of specimen holders.

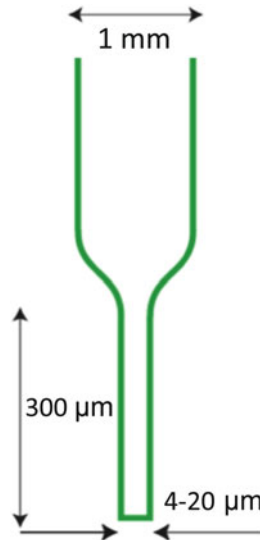


Fig. 2. Dimensions and geometry of a capillary specimen holder.

The “missing wedge” is at best a frustration that causes an unavoidable artifact in the tomographic reconstruction. At worst, this incompleteness in data makes segmentation difficult and interpretations ambiguous. Capillary specimen holders are made from glass or quartz tubes that have had one end pulled to a diameter of 2–10 μm, and have a length of more than 300 μm suitable for being imaged in the soft X-ray microscope, see Fig. 2.

3.1.2. Adding Fiducial Markers to Capillary Specimen Holders

In order to align the images to a common frame of reference (see section below), it is beneficial to coat the capillary specimen holders with 100 nm gold fiducial markers, prior to loading them with cells. This can be done easily using commercially available gold nanoparticles.

1. To coat the capillary specimen holder, simply dip it in the solution of 100 nm gold nanoparticles and slowly withdraw.
2. While the outside of tube is being coated, gently blow air through the capillary to prevent the solution from getting inside.

3.1.3. Specimen Preparation

Prior to being imaged using SXT, lower order cells do not require any special preparation. Indeed, cells such as prokaryotes or yeast can simply be taken from their growth chamber and pipetted directly into a specimen holder and then mounted in the soft X-ray microscope. In some cases the growth media is very high in carbon and nitrogen, and it may be advantageous to transfer the cells into phosphate-buffered saline solution; however, this is not a prerequisite.

For higher order mammalian cells, particularly adherent cells, more care must be taken to ensure the good health of the cells

when they are imaged. In general, we have found the following protocol to produce the best results when imaging adherent cells.

3.1.4. Thawing Adherent Cells to Plating

1. Remove a mammalian cell stock vial from liquid nitrogen temperature storage. If the vial has been submerged in nitrogen, assume nitrogen has seeped into the vial and do not allow it to warm in your hands. Touch the vial as little as possible and always point the cap away from you and others. Place the vial in a preheated 37°C water bath and allow it to thaw for 2–2.5 min. Do not allow the cells to stay at 37°C once the vial is thawed.
2. The outside of the thawed vial is sterilized by dunking, spraying, or dripping with 70% ethanol. Open the vial under sterile conditions and transfer the contents to preheated 37°C media. Freshly frozen cells can be fragile so transfer cells slowly into and out of serological pipette and use care to avoid introducing bubbles.
3. Cell number/cm² differs depending on the size of the cell and the particular requirement of cell line but, generally, plate cells at ~15% density in a plastic cell culture plate, dish or flask. Some cell lines may require a surface coating such as fibronectin, laminin, etc.; however, the actual plating density and surface of growth is cell line specific, and must be determined on a case-by-case basis.

3.1.5. Suspending Adherent Mammalian Cells

Prior to being imaged, adherent mammalian cells are suspended in solution. Once suspended, adherent mammalian cells are treated identically to prokaryotes or lower order eukaryotes, such as yeasts.

1. Filter trypsin, media, and soybean trypsin inhibitor using a 0.2 µm filter to remove debris or other particulate matter.
2. Use trypsin to detach adherent cells for loading into a sample holder (see Note 4). In our hands, we see the best results when cells are detached from plates that are 75–80% confluent.
3. Generally, for a 75 cm² flask, aspirate media, then quickly wash serum from the cell layer with 3 mL of 0.25% trypsin and aspirate wash. Add back 1 mL 0.25% trypsin, distribute, and incubate at 37°C for 2 min or until cells move when the plate is tilted.
4. Stop trypsin by adding 10 mL of media containing 10% serum.
5. Pellet cells by centrifugation (0.3 rcf for 4–10 min) and resuspend the pellet in 400 µL to 1 mL of media.

3.1.6. Specimen Loading in Capillary Sample Holders

Cells must be loaded into the narrow, drawn region of the specimen holder and debris must be kept to a minimum. To help achieve selection of single cells and to minimize debris, size selection via fluorescence-activated cell sorting (FACS) or filtration

is recommended. Filtration by size is described below; discussing FACS of cells is out of the scope of this chapter and may be a protocol that needs to be carried out at a specialist resource, depending on availability.

1. Using a clean air source, blow air into filters and Eppendorf tubes to remove debris, and filter all liquids using a 0.2 μm filter.
2. Construct filter set-ups by gluing (Dow Corning RTV Sealant 732) 1.5 cm^2 squares of BioDesign Cellmicrosieve (20 and 15 μm) onto halved p1000 pipetman tips that have been cut in half to remove the pointed tips. Fit the filter set-ups into 1.5 mL Eppendorf tubes and transfer suspended cells onto filters. Selection for size is done by centrifugation (0.2 rcf for 10 s) using first 20 μm , then 15 μm filters.
3. After final filtration, remove filter set-ups from Eppendorf tubes and pellet cells (0.3 rcf for 4 min). For efficient loading, a high cell titer is recommended. Resuspend the pellet into a volume of loading media (usually growth media) that is 1 \times to 2 \times volume of the pellet.
4. To load cells into a glass capillary tube, add 0.98 μL of high titer cell solution into a microloader tip. Thread the microloader tip into the back end of a capillary tube, place the tip of the microloader in the region of the capillary tube where the glass begins to taper into the portion that has been pulled to a diameter of between 2 and 10 μm and dispense fluid. About 0.1 μL of fluid will fill the pulled tip.
5. Under a brightfield light microscope (10 \times or higher magnification air lens), check that cells are in the region of the glass capillary tube where the sample holder has narrowed to 15 μm or less in diameter. Remove any moveable fluid from the sample holder.
6. Capillary sample holders with cells spanning a 2–10 mm region along its length are ready to be rapidly frozen at the beamline or plunge frozen for later imaging.

3.1.7. Cryofixation

There is a significant amount of literature from the electron microscopy community on cryofixation (20–23). Because SXT imaging is carried out with lower spatial resolution than electron tomography (i.e., 50 nm rather than a few nm), and with X-rays rather than electrons, not all of the commonly accepted “rules” for cryofixation developed by electron microscopists apply (see Note 5). In practice, for soft X-ray tomography success has been achieved with each of two different approaches to cryofixation: cryogenic gas streams and plunge freezing.

1. First, set up a cryostage in the soft X-ray tomography instrument to maintain the sample at near liquid nitrogen temperature

with a stream of cryogenic helium gas at atmospheric pressure (this is the set up of the XM-2 instrument at the ALS in Berkeley).

2. *First approach to freezing: Cryogenic gas stream.* Mount the sample on the sample stage so that it is outside of the cryogenically cooled region, and then quickly plunge the sample into the cryogenically cooled stream of cold helium gas. The sample is then maintained in the stream of helium gas for the duration of the experiment.
3. *Second approach to freezing: Plunge freezing.* Quickly plunge the sample into cryogenic liquid such as liquid propane, liquid ethane, or any other suitable media. In principle, this approach can be straightforward, to the extent that the capillary can be simply plunged manually into the cryogenic liquid. However, to maintain consistency, and allow the speed of plunging to be controlled, it is better if this process is carried out using instrumentation that can vary the speed with which the capillary enters the liquid. Moreover, the plunging time is specimen dependent. For some specimens the time taken to plunge into cryogen is unimportant, for others it is essential that the specimen is plunged as quickly as possible. One difficulty with this technique is maintaining the specimen at cryogenic temperature whilst it is being transferred from the cryogenic liquid onto the sample cryostage of the X-ray microscope; this requires the use of a cryotransfer device. In practice, this can be challenging, and is an additional potential cause of damage to the specimen, if the transfer device is inadvertently allowed to warm up during use. The development of new plunge methods and instruments is very much a work in progress.

In either of these approaches, the final result of the procedure is that the specimen has been loaded into a cryogenically cooled helium gas stream, and is held in place by a spring-loaded clip attached to a motion control stage. At this point, data collection can begin.

3.2. Soft X-Ray Microscopic Data Collection

In the following sections we will describe data collection using the soft X-ray microscope XM-2 located at the Advanced Light Source (ALS), Berkeley. However, the basic principles and concepts will apply to data collection using any soft X-ray microscope.

3.2.1. Aligning the Specimen in the Microscope

The previous section described the process of mounting the specimen in a capillary holder, and cryocooling the sample, typically in situ in the XM-2 cryorotation stage. When the sample is being cooled using the gas method (most common for cells less than 5 μm in diameter), an alignment step is performed after the sample is mounted but before it is cooled. Using the plunge freezing method, the capillary is aligned off-line prior to mounting.

Alignment places the tip of the capillary such that the region to be imaged is centered on the axis of rotation. This is an important step. During tomographic data collection the specimen is rotated by 180° ; during which the specimen should not leave the field of view. The specimen will stay in the field of view during this rotation only if it is centered on the axis of rotation.

1. To perform this alignment, the sample is positioned at 0 and 180° , and the position of the tube is recorded. A tip-tilt stage controlled by a joystick is used to adjust the capillary such that it splits the difference between its positions at the two angles. This procedure is repeated for the tube when positioned at 90 and 270° . Typically, two rounds of alignment are performed to confirm that the tube is exactly centered, especially in the case of large tubes (greater than $8\ \mu\text{m}$) that nearly fill the field of view.
2. The capillary is then lowered quickly into the cryogenic gas stream.
3. Once the tube is aligned and lowered into position for X-ray imaging, the tip-tilt alignment procedure is repeated a final time at finer resolution using X-ray imaging, usually using a region above or below the sample of interest to reduce the X-ray dose on the sample to be imaged.

3.2.2. Tomographic Data Collection

1. Look for fields of view that contain cells of interest for the given experiment. Projection images are taken along the length of the capillary. This allows the position of the optimal fields of view to be identified.
2. Set up a tomography scan. In the XM-2 control GUI, sample description is saved in a header file along with the image data; this information is also transferred into the image database. The parameters for the scan are also selected: exposure time, angular increment and total angular range. Exposure time is chosen such that the CCD receives the maximum number of counts without saturating (also known as clipping) any pixels, generally around $100\ \text{ms}$ on this microscope. The angular increment is generally between 1 and 2° , for a total number of images between 90 and 180 , spread over 180° .
3. After the scan is started, continue observing the sample. In rare cases, drift leads the specimen to leave the field of view during the scan. In this case, slightly adjust the horizontal or vertical position between images to re-center the sample in the field of view. Obviously, this adjustment should be timed so that it is not carried out during acquisition of an image.
4. Collect a set of “flatfield” images before and after tomographic image data are recorded. To do this, move the capillary out of the field of view, and collect a series of 10 – 20 images. By combining these images with the sample images from the tomogram,

the percent transmission can be calculated, yielding quantitative X-ray absorption data.

5. Data for a completed tomographic set is saved as 16 bit unsigned tiff stacks. There are a total of three files: one with the initial flat fields, one tomography image series, and one with the final flat fields.

3.3. Data Processing

3.3.1. Image Correction and Normalization

1. As the first step in processing the images, subtract the detector dark counts from both the sample images and the flat field images. The dark counts can be measured by collecting an image with the X-ray shutter closed. The dark field image only needs to be measured every few months; our experience is that it does not change on this time scale.
2. After subtracting the dark counts, average each of the two sets of flat field images to produce a single initial flat field image and a single final flat field image. Average multiple flat fields to reduce the noise level.
3. Divide the first half of the images in the tilt series by the initial averaged flat field image, and divide the second half of the images in the tilt series by the final averaged flat field image. In other words, the value of each pixel in the sample image is divided by the value in the corresponding pixel of the flat field image, and the resulting value is placed in the corresponding pixel of the output image. This results in a stack of images corresponding to the percent X-ray transmission through the sample over the series of angles recorded.
4. Before going to the next step (image alignment), correct for dead pixels on the CCD. These are pixels that read out very low counts regardless of the X-ray flux on them. To carry out this correction requires a pixel-by-pixel map identifying each bad CCD pixel. For each image in the series, the bad pixels are replaced by a value interpolated from the surrounding pixels. We use a program from the IMOD package called CCDERASER to perform this step.
5. Finally, down-sample the images from $2,048 \times 2,048$ to $1,024 \times 1,024$ using a simple binning strategy. This is done to reduce the extent of unnecessary oversampling: the resolution of the experiment is approximately 50 nm (based on the zone plate outer ring radius), but the pixel size at $2,048 \times 2,048$ is approximately 8 nm. By reducing the image size to $1,024 \times 1,024$, the pixel size is increased to 16 nm, which is still sufficiently small enough to capture all relevant detail in the images.

In practice, these calculations have been implemented both as a MATLAB script and an ImageJ plugin. Either of these implementations can be used to carry out this step, yielding identical output in

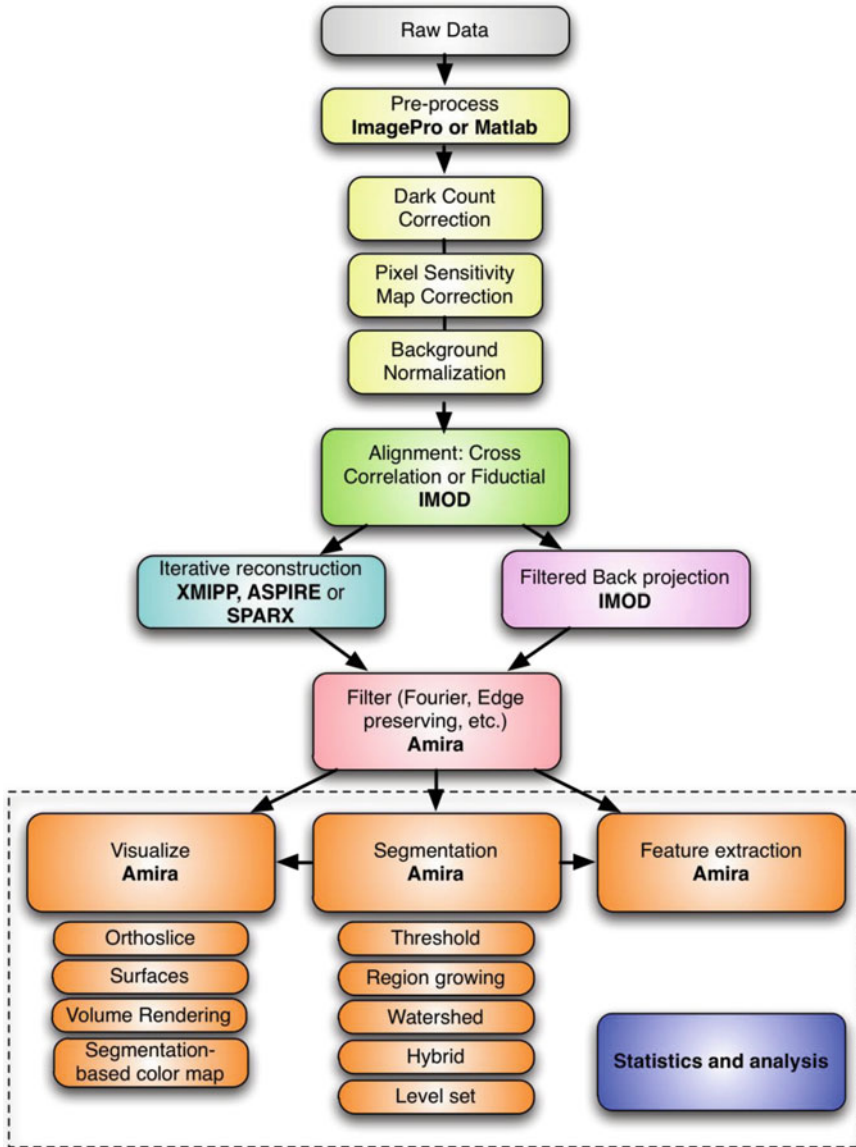


Fig. 3. A flowchart showing the steps and software packages required to process raw imaging data from XM-2, and to calculate, visualize and segment 3-dimensional reconstructions.

a similar amount of time (the bottleneck is mainly reading from and writing to disk). In both cases, versions of the script or plugin can be run in which an entire directory of images can automatically be processed. In Fig. 3 we show the software packages in common use by users of XM-2, together with their relative sequence of use and the functions performed. Naturally, this list of software is organic, and liable to change as new, improved algorithms become available, or when experimental need dictates use of other software.

3.3.2. Image Alignment

Because of imperfections in the specimen rotation stage, the sample appears to “jump” in position (x and y translation as well as rotation in the plane of the image) from one frame to another. The images in the projection image series must, therefore, be aligned to bring them into agreement within a single frame of reference. From the perspective of a user of the soft X-ray tomography instrument, the two approaches to this are to rely on the automated methods that have already been implemented, or to manually align the images by tracking the fiducial markers (the gold nanoparticles which were added to the outside of the capillary tubes). These methods will be described below. While automated alignment can give results quickly and with no human interaction, as of this writing, the quality of the alignment given by automated methods does not always match that given by manually tracking fiducial markers. Thus, in practice the automated approach is often used to guide decisions during an experiment and give initial results. However, when a higher quality alignment is required, manual fiducial alignment is typically required.

3.3.3. Automated Alignment

A number of automated alignment approaches have been published. At XM-2, a robust approach has been implemented and recently submitted for publication (Parkinson et al. *J. Struct. Biology*, submitted). First, each image in the projection stack is aligned to the projection images from adjacent angles by cross correlations. In the words of the IMOD software package, this allows the construction of a coarsely aligned projection image stack by applying transforms to the original images. Second, the position of the center of rotation with respect to the images is determined. Third, an initial tomographic reconstruction is generated. Fourth, at each angle at which a projection image was collected in the original data set, a re-projection is generated from the reconstructed 3D model volume. Fifth, these re-projections are compared with the original projection images, and the transform needed to align each original projection to the re-projection from the model at that angle is refined. Finally, steps three through five are repeated iteratively. On each iteration the reconstructed volume should improve as the alignment errors decrease. This process is generally termed “model-based alignment”.

In practice at XM-2, a user types a single command in MATLAB, with the file name of the normalized image stack as the input parameter (alternatively, an entire directory of files can be automatically aligned). The MATLAB distributed computing toolbox is used, running on a 20-node Mac cluster, which increases the speed of the process. Typically, it only takes seconds to minutes to carry out this stage.

3.3.4. Fiducial Alignment

For manual alignment of fiducial markers we recommend the IMOD software package. Their Web site has extensive documentation

and tutorials on this software. We note a few important details specific to soft X-ray tomography using capillary tubes, and which are not extensively covered in the IMOD tutorials.

1. In the coarse alignment phase (which is similar to the cross-correlation stage of automatic alignment, described above), check the box for “cumulative correlation” along with the box for “no cosine stretch”.
2. When creating the seed model, avoid attempting to mark gold fiducial markers when they are at the edges of the tube—it is too difficult to accurately mark them in these regions. We have found that in soft X-ray microscopy the gold fiducial markers are of much lower relative contrast with respect to the surrounding sample than in electron microscopy. This is due in large part to the thickness of the samples in SXT compared to those imaged with EM. This is especially true at the extreme left and right edges of the tube, where the X-rays pass nearly tangent to the tube edge and thus transmit through more glass or quartz material.
3. In a similar vein to step 2, during fiducial model generation, avoid tracking the seed model or filling model gaps. Automatic tracking generally fails in these regions, and leads to worse overall alignment.
4. The more fiducial markers, the better the alignment. We pick a minimum of six markers, if available, which is much less than recommended by IMOD, but which we have found, nevertheless, gives a good alignment.

3.4. Tomographic Reconstruction

In the reconstruction step, a three-dimensional volume is produced based on the stack of aligned projections. There are a number of algorithms used to carry out this step, and this is very much an active area of research. In terms of the differences apparent to the eye, the methods mainly differ in the amount and type of noise and/or artifacts present in the final reconstruction, and in the smoothness or sharpness of object boundaries in the image. The goal of all of these methods is to give the minimum amount of noise, while still preserving all relevant image detail, including sharp edges (sometimes referred to as resolution). The challenge is that, in general, methods that reduce noise in the image also reduce resolution. The compromise that is reached between noise and resolution generally depends on what subsequent processing will be applied to the reconstructed volume. If digital slices through the volume are going to be directly visualized, different settings have been found to be optimal as compared to the case when volumes are going to be automatically segmented. The two main classes of reconstruction algorithms can be classified as Fourier methods and real-space methods, and will be briefly described below, followed by a description of their practical implementation and the comparisons between them.

3.4.1. *Fourier Methods*

The most common method in this class is known as filtered backprojection. It relies on the central slice theorem, and is implemented by Fourier transforming each image in the original stack, filtering it, performing an inverse Fourier transform, and “backprojecting” this filtered image across the volume to be reconstructed, interpolating appropriate values for all the voxels. By combining the backprojections from all of the various orientations, a final volume is reconstructed. Two strengths of this algorithm are that it is computationally fast, and it gives a unique result for a given type and level of filtering.

3.4.2. *Real-Space Methods*

In real-space methods, individual images are iteratively compared directly with the reconstructed volume, and the volume voxels are updated to bring them into better agreement with the values expected. There are a large number of strategies for how to perform this update and carry out the iterations. There are also a number of constraints that can be added during the iterations, including a requirement that all voxels must have values greater than or equal to zero (corresponding to no voxels having a physically impossible “negative transmission”). In addition, there are a number of ways to add smoothing, or regularization, to the result—for example, when updating the voxels, a penalty term can be added which encourages adjacent voxels to have similar, rather than different values. This penalty term can be made nonlinear, in an attempt to both encourage sharp edges (high resolution) while reducing noise.

A particular strength of iterative methods is that they have been shown in the literature to give the optimal tradeoff between noise and resolution. This is especially true for the relatively low number of projections used in soft X-ray tomography. In addition, iterative methods have the advantage of being able to include additional constraints, which can improve the accuracy of results. One drawback of iterative methods is that they are computationally intensive, and thus can be very time consuming in the absence of significant computational resources.

3.4.3. *Reconstruction in Practice*

A number of iterative and Fourier reconstruction methods are available to users of XM-2 through MATLAB scripts which take advantage of the 20-node cluster and the MATLAB distributed computing toolbox. The reconstructions are run by typing a single command, with inputs to indicate the selected reconstruction method, and the type and level of filtering (or regularization). Reconstructions by Fourier methods are complete in 1 min or less; reconstructions by iterative methods generally take 10–20 min to complete. Thus, for data that will be analyzed in depth in subsequent steps, users sometimes perform reconstructions with a series of methods and filtering levels to determine which best meets their needs. A challenge in comparing Fourier and real-space methods is

that each method has a different approach to achieving the optimal tradeoff between noise and resolution. In addition, the original images can be filtered prior to carrying out the reconstruction, which also affects the final result. Thus, rather than to try to give a detailed comparison, we will make a few general observations:

1. Iterative methods give a clear advantage in terms of reducing “streaking” artifacts due to the presence of gold fiducial markers. Using filtered backprojection, we often find streaks coming off of these markers in one or more directions; these streaks are significantly reduced using iterative methods.
2. Iterative algorithms which use nonlinear regularization to implement edge-preserving smoothing during the reconstruction process can give volumes which are more readily segmented using automated methods, whereas volumes from filtered backprojection must be filtered by other methods before performing automated segmentation. Distinguishing which of these methods provides more accurate results for real data is difficult, and must be assessed on a case to case basis.

3.5. Visualization

A number of commercial, academic, and open source software packages are available for visualizing tomographic reconstructions (see Subheading 2). Amira is our preferred tool; we note that Avizo uses much of the same code base as Amira, and has similar capabilities. In this section, we will describe our workflow in Amira, but similar results can be achieved with other tools.

1. First load reconstructions into Amira. Correctly set the voxel size to the appropriate units; for example, in many cases we use volumes where the voxel size is 32.7 nm on each side. The volume is then visualized in the form of one-voxel-thick digital slices through the volume (known as “orthoslices” or “oblique slices” in Amira; Fig. 4a, b). These allow for viewing of exterior and interior portions of a volume from any arbitrary axis.
2. Adjust the contrast of the orthoslices in order to discern subtle subcellular features, for example, to help delineate the boundaries between organelles and the cytosol, or between structures inside a particular cellular space. An examination of the orthoslices is a relatively quick way to determine the cellular characteristics of the reconstructed cells, for example, to determine the condition of the cells or their stage in the cell cycle. Inspection of the orthoslices also allows for a quick comparison between control cells and variable cells. This facilitates efficient screening of the reconstructions, allowing good reconstructions with useful information to be chosen for segmentation. Since manual segmentation can be very time consuming, being able to select only the optimal reconstructions increases the efficiency of data analysis.

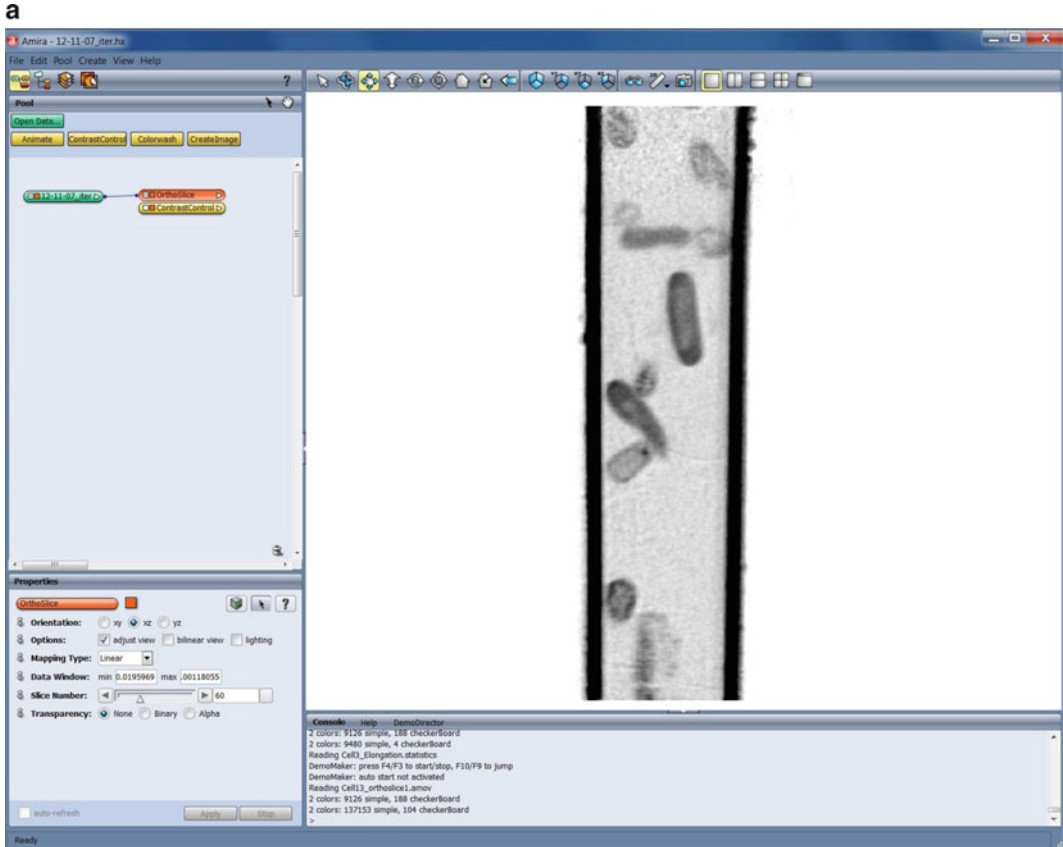


Fig. 4. Screen captures showing commonly used tools in the visualization software package Amira. (a) The viewer panel on the right hand side is being used to view a single orthoslice through the reconstructed field of view (in this case, this is a reconstruction of a capillary tube filled with a suspension of bacterial cells). The vertical thick black lines are from the capillary tube. Darker regions represent areas with a relatively high LAC compared to lighter regions. (b) When carrying out the process of segmentation it is usually beneficial to view the reconstruction from orthogonal angles. *Top half* and *bottom-left* quadrant of the viewing panel shows three slices through the reconstruction. *Bottom right* quadrant shows 3D representation of segmented cells. (c) View of the “magic wand” tool being used to select regions inside the cells with similar LAC values. (d) Using the “paintbrush” tool to edit the region selected with the “magic wand” shown in (c), (e) The “lasso” tool is an efficient means of isolating regions of interest in the reconstruction. For example, you could use it to isolate one cell from other cells reconstructed in the same field of view. (f) One example of visualizing the segmented data set. Purple represents the transparent outer surface of the cells. Orange represents the internal structures of interest.

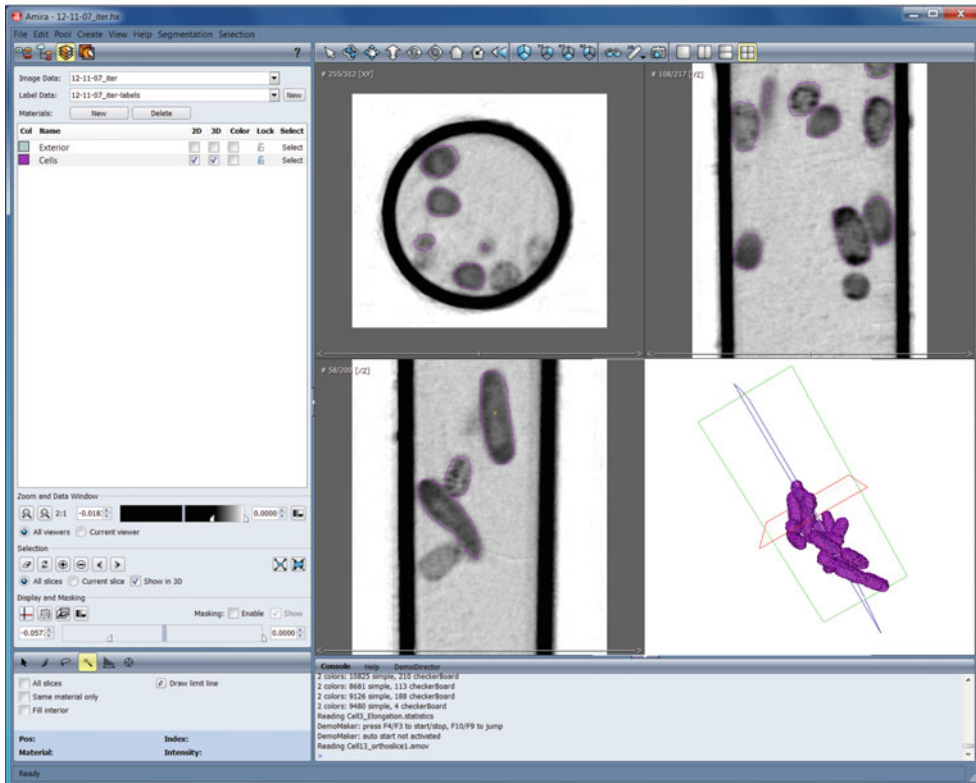
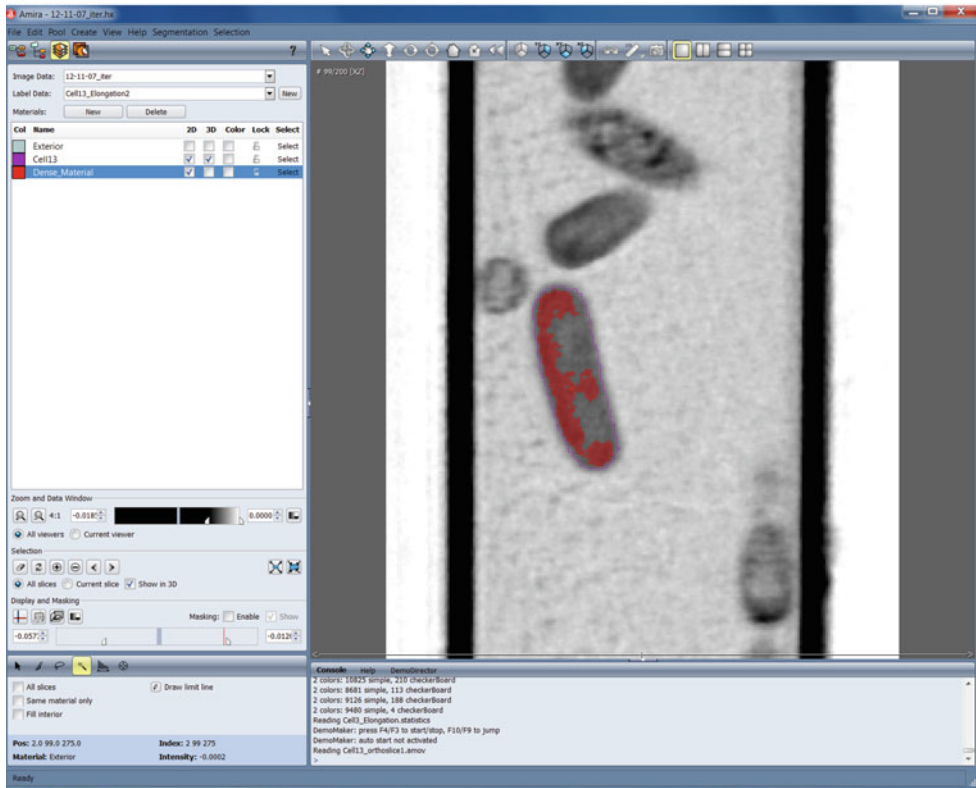
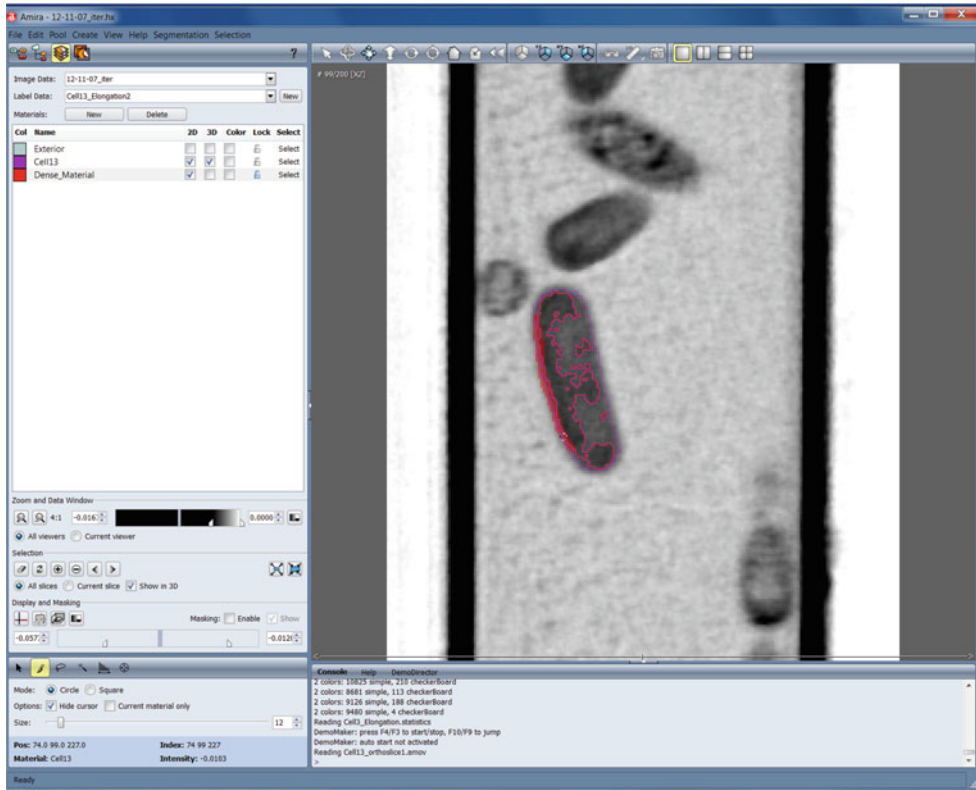
b**c**

Fig. 4. (continued)

d



e

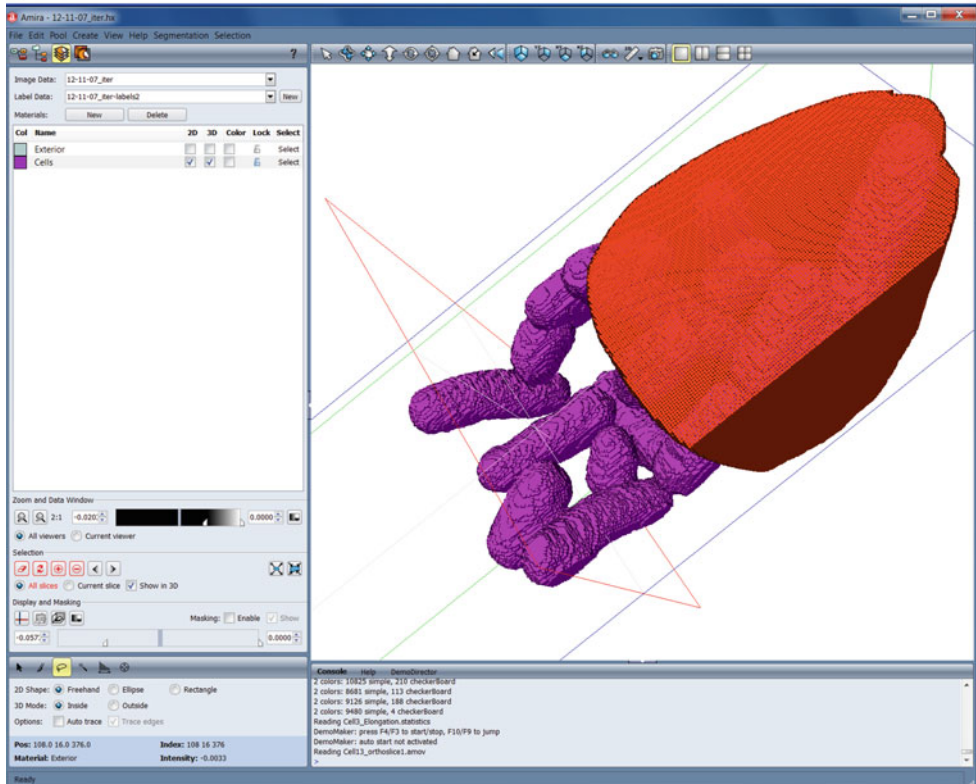


Fig. 4. (continued)

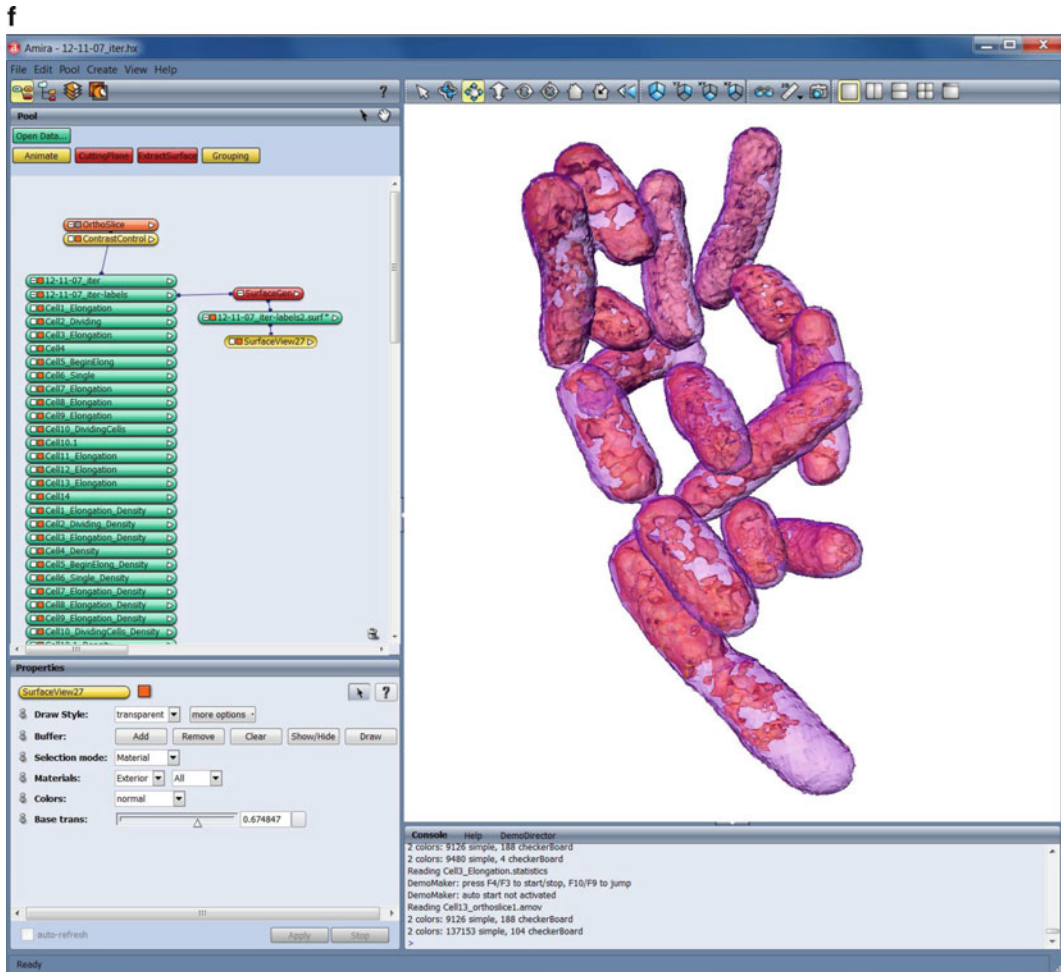


Fig. 4. (continued)

3.6. Segmentation and Analysis

The purpose of segmentation is to delineate the boundaries of structures of interest. Segmentation serves as a way to isolate a specific cellular component from the data set, allowing 3-dimensional visualization of that component either alone or with other components. This segmented region can serve as the basis for a representation of a whole cell, organelle, or some other specific structure that has been selected for analysis.

Two factors serve as the basis for segmentation of cellular structures. First, different structures differentially attenuate X-rays, and thus boundaries between structures can often be found on the basis of changes in voxel values (corresponding to different X-ray attenuation). Sometimes, cells or organelles to be segmented have uniform X-ray attenuation, and thus regions of interest are separated from each other based on attenuation alone. In other cases, a second

factor must be used: knowledge of the expected structure of the items to be segmented. For example, some organelles often have complex shapes, and are composed of subregions with different X-ray attenuations. Thus, these organelles must be segmented not only based on attenuation, but also based on prior information about expected shapes.

Segmentation of areas of interest within the cell can be performed manually using image manipulation with tools such as a “magic wand” (Fig. 4c), “paintbrush” (Fig. 4d) and “lasso” (Fig. 4e). The magic wand function is used as a region-growing tool, where the user picks a seed point as well as an upper and lower threshold; all voxels connected to the seed point that fall within the threshold are added to the region. The magic wand can function either in 2D or 3D. With the paintbrush tool, a user paints regions of interest on a slice-by-slice basis. In order to create a 3-dimensional representation of a cellular component, each portion of the component must be selected on each orthoslice. After performing initial paintbrush segmentation by selecting through slices along one axis, it is important to view the selected components in an orthogonal axis to confirm the continuity and accuracy of the selected region in 3 dimensions. Efforts must be taken to reconcile the regions that can be viewed in each axis. Amira can also show a 3-dimensional view of the currently selected voxels, which can aid in determining the accuracy of segmentation; for example, many organelles should have relatively spherical shapes, and the 3D view of the segmentation should conform to this. Segmentation must be recorded in some way; in Amira this is done by means of a “label field”. Label fields are used to assign a unique identity to each voxel in a volume. Label fields can then be used as a mask for the original volume or can be used as the basis for a 3D surface representation (Fig. 4f).

Although segmentation of complex biological samples often needs to be done manually, it is possible to automate the process in some cases. In fact, the magic wand tool could be viewed as a semi-automatic segmentation method. If the difference in X-ray attenuation between a given structure and its neighbors is relatively large, the magic wand can be fast and accurate. In other cases, or in cases of samples with high levels of noise, selecting appropriate thresholds is more difficult; often a smaller threshold range must be used to prevent bleed-through of the selected region to the surrounding structures. This adjustment of the threshold in turn changes the overall selected volume. Thus, the ability to arbitrarily adjust the thresholds is very useful but can lead to highly subjective results if segmentation is being used as the basis for volume analysis.

A number of more automatic segmentation methods are possible, however, we have found that automated image processing “pipelines” must have a number of parameters very specific to a given problem. Unless a number of cells or organelles are being

analyzed, finding and testing appropriate algorithms and then setting up the “automatic” pipeline can take longer than manually performing the segmentation.

With semi- or fully automatic segmentation, it is often necessary to go through orthoslices in each axis and make small corrections to the given selection. The paintbrush, with that ability to adjust the brush size, has proven to be useful for subtracting or adding voxels to a selection. While corrections can be time consuming, we have found that the use of a pen tablet by Wacom can make this process more efficient. Pens are useful precision tools that tend to be easier to manipulate than a mouse. Additionally, a tablet is able to provide more screen space for segmentation and the angle of display can be adjusted based on user preferences. The work environment can be further personalized using adjustable ergonomic products from companies such as Ergotron (<http://www.ergotron.com/>). We have used these products to mount and mobilize tablets so that different users can configure their workspace optimally. We have found that ergonomics are an important factor in the segmentation process. Improving workstation ergonomics greatly improved the productivity and throughput of this frequently laborious task.

When selecting structures that are close to one another or that overlap, it can be useful to segment the structures in different label fields. This is because any given voxel in an orthoslice can only belong to one material in a given label field. Selecting a voxel for a certain material that has already been selected will remove the voxel from the original material. This could create inaccuracies in the representative 3-dimensional volume. For example, one label field could contain the overall cell, while another could contain information about the organelle boundaries, and a third could contain information about sub-organelle structure.

In order to visualize the segmentation results for a certain material in 3-dimensions, a surface must first be generated. There are a number of methods of surface generation. In Amira, an important option is the amount of smoothing that is applied in the generation of the surface. The constrained smoothing option works well for most specimens, especially for components with detailed structures. Once a surface has been generated, it can be viewed in the viewer window. Any number of surfaces representing different materials can be displayed simultaneously in the viewer window. The method used for displaying the surfaces can have a big impact on the final product. In Amira, under the “more options” section of the “draw style” parameter on a Surface View module, the default is to use “triangle normals.” We have found that the surfaces are much more pleasing when “vertex normal” is selected; this prevents the surface from showing the corners of the individual voxels in the segmentation. The surface area function will generate a spreadsheet that displays the volume and surface area of a certain

material in voxel units. The material statistics function can also be used to directly calculate the volumes from the label field. If the voxel size was appropriately set when a data set was loaded, the volume and surface area values will be in the appropriate units (in our case, we use cubic or squared microns).

We note that because data is measured in terms of percent transmission, if appropriate reconstruction algorithms are used, the voxel values in the final volume correspond to the average value of the linear absorption coefficient (LAC) for the material in that voxel. In some cases, it may be necessary to scale the values in the volume by some conversion factor so that they correspond to appropriate units—in X-ray microscopy; absorption per inverse micrometer is a common measure.

4. Notes

1. A wide range of computing hardware can be used to run tomographic reconstruction and analysis software packages. However, as with most computationally intensive operations, access to more/faster CPUs will result in a reduction in the time it takes to process and analyze data. At XM-2, data are currently processed and analyzed using an Apple cluster with 20 nodes, each with two 2-core processors. In the near future, it appears these types of calculations will be best carried out using GPU clusters (Graphical Processing Units) as these typically produce a significant decrease in processing time (a factor of 20 or more is generally expected for this type of calculation). However, at a push tomographic reconstruction using the filtered backprojection algorithm can even be carried out on a modest laptop. Therefore, computational hardware is mostly determined by availability of funding, and required throughput.
2. Much of the pre- and post-processing can be done using commonly available commercial software packages such as MATLAB (Mathworks) or with the freeware package ImageJ (National Institutes of Health, USA; <http://rsbweb.nih.gov/ij>). Tomographic reconstructions can also be carried out in MATLAB or in ImageJ using readily available plugins. There are also a number of dedicated tomography software packages, and in our hands we have found these to offer some distinct advantages, such as utilities for the correction for bad CCD pixels (CCDERASER in IMOD). Many of the required computational operations can be combined into one automated “pipeline” using either a MATLAB script or an ImageJ plugin; this saves time and makes it relatively easy for a neophyte to process their own SXT data. For the calculation of iterative reconstructions we use a number of different packages, including XMIPP

(<http://xmipp.cnb.csic.es/>), ASPIRE (<http://www.eecs.umich.edu/~fessler/aspire/>), and SPARX (<http://macro-em.org/sparxwiki/SparxWiki>). We recommend flexibility in terms of software packages. Some packages deal with particular data sets better than others (based on how the algorithm handles noise, aberrations, and other inherent features in the data). For best results, it is usually worthwhile to carry out data processing and analysis in parallel using different software packages, and compare the final products to determine which performed best with that particular specimen/data set.

3. Amira™ (Visage Imaging, Germany) and Avizo (VSG, France) are two examples with similar functionality. Additional software packages include ImageJ, Chimera (University of California in San Francisco, USA), IMOD (University of Colorado, USA), VisIt (Department of Energy: Advanced Simulation and Computation Initiative, <https://wci.llnl.gov/codes/visit/>), Paraview (Kitware, Inc., <http://www.paraview.org/>), and VG Studio Max (Volume Graphics). The choice of package (between these, and many others available either commercially or freely) depends on funding and preference. For the most part, any of the modern software packages are sufficiently advanced and can meet most needs; choice comes down to one of individual preference, perceived ease of use, and other similar considerations.
4. The actual strength of trypsin used is cell line dependent as is the method of stopping action of trypsin. Some cell lines require lower strength of trypsin, for example 0.10%, and may require non-serum stops such as soybean trypsin inhibitor (Sigma Aldrich). To achieve cells in suspension, balance exposure to trypsin with the morphology of cells. Longer trypsin exposure detaches more cells but also negatively affects cell viability and morphology. Also, do not use forceful pipetting, knocking, or scraping to detach cells. Fast liquid movement, knocking and scraping can shear cells, producing debris that may be difficult to separate from desired samples.
5. SXT is a relatively straightforward imaging technique, and comparatively free of issues once the cells are mounted in a suitable holder and cryofixed. The primary concern is always the authenticity of the specimen—is the reconstructed cell a true and accurate representation of the *in vivo* state. Therefore, we encourage the use of correlated imaging methods, both as a source of additional information and as a “reality check.” Towards this end we have developed high-numerical aperture cryogenic light microscopy, and installed this instrumentation into XM-2 (9, 24). As a result, fluorescent tagged-molecules or structures in the cells can be imaged using fluorescence microscopy prior to the cells being imaged using SXT. By fluorescently tagging subcellular structures with well-established

architecture—such as the mitochondria in yeast—and comparing room temperature fluorescence imaging data with the patterns seen in cryogenic light and X-ray microscopy it is possible to validate the integrity of the cell after cryofixation, and after SXT data collection. We feel this is enormously important and this correlated approach should be a routine part of imaging cells by any high-resolution modality. We have observed a number of dramatic structural changes that we determined were simply due to poor freezing, or other specimen handling protocols. In the absence of correlated imaging data these changes could easily have been attributed as being biologically significant.

Acknowledgments

XM-2 and associated research is funded by the Department of Energy Office of Biological and Environmental Research Grant DE-AC02-05CH11231, the NIH National Center for Research Resources (5P41 RR019664-08) and the National Institute of General Medical Sciences (8P41 GM103445-08) from the National Institutes of Health.

References

1. Larabell CA, Nugent KA (2010) Imaging cellular architecture with X-rays. *Curr Opin Struct Biol* 20:623–631
2. Leis A, Rockel B, Andrees L, Baumeister W (2009) Visualizing cells at the nanoscale. *Trends Biochem Sci* 34:60–70
3. Fagarasanu A, Fagarasanu M, Rachubinski RA (2007) Maintaining peroxisome populations: a story of division and inheritance. *Annu Rev Cell Dev Biol* 23:321–344
4. Warren G, Wickner W (1996) Organelle inheritance. *Cell* 84:395–400
5. Uchida M, Sun Y, McDermott G et al (2011) Quantitative analysis of yeast internal architecture using soft X-ray tomography. *Yeast* 28:227–236
6. Baumeister W (2002) Electron tomography: towards visualizing the molecular organization of the cytoplasm. *Curr Opin Struct Biol* 12: 679–684
7. Natterer F (1986) *The mathematics of computerized tomography*. Wiley, New York
8. Larabell CA, McDermott G, Le Gros MA (2005) X-ray tomography of whole cells. *Curr Opin Struct Biol* 15:593–600
9. McDermott G, Le Gros MA, Knoechel CG, Uchida M, Larabell CA (2009) Soft X-ray tomography and cryogenic light microscopy: the cool combination in cellular imaging. *Trends Cell Biol* 19:587–595
10. Uchida M, McDermott G, Wetzler M et al (2009) Soft X-ray tomography of phenotypic switching and the cellular response to antifungal peptoids in *Candida albicans*. *Proc Natl Acad Sci USA* 106:19375–19380
11. Attwood DT (1999) *Soft X-rays and extreme ultraviolet radiation: principles and applications*. Cambridge University Press, New York
12. Weiss D (2000) *Computed tomography based on cryo X-ray microscopic images of unsectioned biological specimens*. Georg-August University of Göttingen, Göttingen
13. Le Gros MA, McDermott G, Larabell CA (2005) X-ray tomography of whole cells. *Curr Opin Struct Biol* 15:593–600
14. Parkinson DY, McDermott G, Etkin LD, Le Gros MA, Larabell CA (2008) Quantitative 3-D imaging of eukaryotic cells using soft X-ray tomography. *J Struc Biol* 162:380–386

15. Larabell C, McDermott G, Uchida M, Knoechel C, Le Gros MA (2009) Imaging whole cells at better than 50 nm isotropic resolution with X-rays. *Abst, Papers Am Chem Soc*, 238
16. Larabell CA, Le Gros MA (2004) X-ray tomography generates 3-D reconstructions of the yeast, *saccharomyces cerevisiae*, at 60-nm resolution. *Mol Biol Cell* 15:957–962
17. Bertilson M, Von Hofsten O, Lindblom M, Wilhein T, Hertz H, Vogt U (2008) Compact high-resolution differential interference contrast soft X-ray microscopy. *App Phys Lett* 92:064104
18. Bertilson MC, Takman PAC, Holmberg A, Vogt U, Hertz HM (2007) Laboratory arrangement for soft X-ray zone plate efficiency measurements. *Rev Sci Instrum* 78:026103–026101
19. Takman PAC, Stollberg H, Johansson GA, Holmberg A, Lindblom M, Hertz HM (2007) High-resolution compact X-ray microscopy. *J Microsc* 226:175–181
20. Bell PB, SafiejkoMroccka B (1997) Preparing whole mounts of biological specimens for imaging macromolecular structures by light and electron microscopy. *Int J Imaging Syst Tech* 8:225–239
21. Quintana C (1994) Cryofixation, Cryosubstitution, Cryoembedding for Ultrastructural, Immunocytochemical and Microanalytical Studies. *Micron* 25:63–99
22. Ryan KP (1992) Cryofixation of tissues for electron-microscopy—a review of plunge cooling methods. *Scanning Microsc* 6:715–743
23. Studer D, Humbel BM, Chiquet M (2008) Electron microscopy of high pressure frozen samples: bridging the gap between cellular ultrastructure and atomic resolution. *Histochem Cell Biol* 130:877–889
24. Le Gros MA, McDermott G, Uchida M, Knoechel CG, Larabell CA (2009) High-aperture cryogenic light microscopy. *J Microsc* 235:1–8